Lithium titanate as anode material in lithium-ion batteries

- A surface study

Licentiate thesis

Tim Nordh

Department of Chemistry – Ångström Laboratory
Ångström Advanced Battery Centre
Uppsala University

Abstract

The ever increasing awareness of the environment and sustainability drives research to find new solutions in every part of society. In the transport sector, this has led to a goal of replacing the internal combustion engine (ICE) with an electrical engine that can be powered by renewable electricity. As a battery for vehicles, the Li-ion chemistries have become dominant due to their superior volumetric and gravimetric energy densities. While promising, electric vehicles require further improvements in terms of capacity and power output before they can truly replace their ICE counterparts. Another aspect is the CO_2 emissions over lifetime, since the electric vehicle itself presently outlives its battery, making battery replacement necessary. If the lifetime of the battery could be increased, the life-cycle emissions would be significantly lowered, making the electric vehicle an even more suitable candidate for a sustainable society. In this context, lithium titanium oxide (LTO) has been suggested as a new anode material in heavy electric vehicles applications due to intrinsic properties regarding safety, lifetime and availability. The LTO battery chemistry is, however, not fully understood and fundamental research is necessary for future improvements. The scope of this project is to investigate degradation mechanisms in LTO-based batteries to be able to mitigate these and prolong the device lifetime so that, in the end, a suitable chemistry for large scale applications can be suggested. The work presented in this licentiate thesis is focused on the LTO electrode/electrolyte interface. Photoelectron spectroscopy (PES) was applied to determine whether the usage of LTO would prevent anode-side electrolyte decomposition, as suggested from the intercalation potential being inside the electrochemical stability window of common electrolytes. It has been found that electrolyte decomposition indeed occurs, with mostly hydrocarbons of ethers, carboxylates, and some inorganic lithium fluoride as decomposition products, and that this decomposition to some extent ensued irrespective of electrochemical battery operation activity. Second, an investigation into how crossover of manganese ions from Mn-based cathodes influences this interfacial layer has been conducted. It was found, using a combination of high-energy x-ray photoelectron spectroscopy (HAXPES) and near-edge x-ray absorption fine structure (NEXAFS) that although manganese is present on the LTO anode surface when paired with a common manganese oxide spinel cathode, the manganese does little to alter the surface chemistry of the LTO electrode.

List of papers

This thesis is based on the following papers, which are referred to in the text by their Roman numerals.

I. **Depth profiling the solid electrolyte interphase on lithium titanate ($Li_4Ti_5O_{12}$) using synchrotron-based photoelectron spectroscopy**
T. Nordh, R. Younesi, D. Brandell, K. Edström
Journal of Power Sources 294, 2015, 173-179

II. **Manganese in the SEI layer of $Li_4Ti_5O_{12}$ studied using combined NEXAFS and HAXPES techniques**
T. Nordh, R. Younesi, M. Hahlin, C. Tengstedt, D. Brandell, K. Edström
Submitted to Physical Chemistry Chemical Physics.

Reprints were made with permission from the respective publishers.

Comments on my contributions to the Papers

I. Planned and performed most of the experimental work (battery assembly, electrochemical tests, PES measurements, and data interpretation). Wrote the manuscript, took part in all discussions.

II. Planned and performed all experimental work and data analysis. Wrote the manuscript and participated in all discussions.

“The quanta really are a hopeless mess”

-Albert Einstein

Contents

Abbreviations

CMC	Carboxymethyl cellulose
DEC	Diethyl carbonate
DMC	Dimethyl carbonate
EC	Ethylene carbonate
ESW	Electrochemical stability window
FEC	Fluoroethylene carbonate
HAXPES	Hard X-ray photoelectron spectra
ICE	Internal combustion engine
IMFP	Inelastic mean free path
LCO	Lithium cobalt oxide
LFP	Lithium iron phosphate
LIB	Lithium-ion battery
LiTFSI	Lithium bis(trifluoromethanesulfonyl)imide
LMO	Lithium manganese oxide
LMNO	Lithium manganese nickel oxide
LTO	Lithium titanate oxide
NCA	Lithium nickel cobalt oxide
NEXAFS	Near edge X-ray fine structure
NMC	Lithium nickel manganese cobalt oxide
OCV	Open circuit voltage
PAA	Polyacrylic acid
PES	Photoelectron spectroscopy
PVdF	Polyvinylidene difluoride
SEI	Solid electrolyte interphase
SPE	Solid polymer electrolyte
VC	Vinylene carbonate
XPS	X-ray photoelectron spectroscopy

1. Introduction

1.1 Lithium-Ion Batteries

The concept of storing energy electrochemically has been known since the discovery of the voltaic pile in the very beginning of nineteenth century. Batteries have provided an excellent source of energy for applications not connected to the grid, i.e. portable devices, or where consumption is separated from production in time, i.e. power storage. With the advent of the automotive industry, the lead-acid battery grew in popularity as an energy source for engine ignition. The robustness of the system and the inexpensiveness of the battery constituents made lead-acid an ideal choice for this application. As shown in Fig. 1a, lead-acid is not the best chemistry in terms of gravimetric or volumetric energy density; there are better performing alternatives[1]. Ni-MH later conquered the market of portable power tools by having high enough power while being light enough for handheld devices. While possessing the best properties in theory, the lithium-based batteries were for many years not real contenders due to price and practical issues of getting a reliably functioning cell. The emergence of a of portable electronic devices such as laptops and mobile phones, however, created a niche in which customers were willing to pay for increased battery performance. This fueled the research on Li-ion batteries (LIBs) to find a working cell chemistry[1,2]. While promising materials had been found both for the positive and negative electrodes already around 1980, it would take until 1991 with the patented work of Asahi Kasei and Sony for a real commercialization of LIBs[3]. Since the launch, LIBs have had an ever increasing market share, not only due to the increased usage of electronic devices but also because growing environmental concerns have pushed the progress of electric and hybrid vehicles forward, creating a whole new market to expand into.

The basic concept of a battery is to have reduction and oxidation reactions which are separated in space, forcing the electrons to move in an external circuit where they can power an electric device. The early batteries utilized an irreversible chemical process rendering them useful for one-time use only, yielding so-called primary batteries. LIBs are built on reversible processes so that recharging is possible after use, and are an example of secondary batteries. Historically, secondary batteries often underwent a pre-cycling at the factory before shipping to consumers, and the ‘primary’ and ‘secondary’ prefixes are thus referring to which cycle the battery is in when arriving to

the consumer. While metallic lithium would yield the highest gravimetric and volumetric capacity, the inherent safety issues with dendrite formation and subsequent short-circuiting forced the implementation of the "rocking chair" type of cells in which intercalation of lithium ions into graphite prevented the dendrite formation[1]. Fig. 1b displays a schematic representation of the basic workings of a secondary battery of a "rocking chair" type. There is a negative electrode (anode) and a positive electrode (cathode) which act as host intercalation materials in which lithium ions shuttle between during charge and discharge. During discharge (normal operation), the ions move from anode to cathode while the direction is reversed during charge (i.e. recharging of the battery).

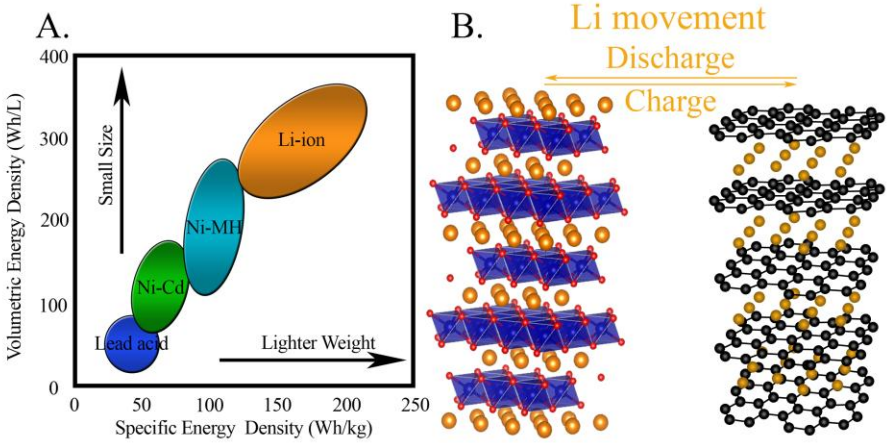

Figure 1. A) A plot showing the specific energy and volumetric energy for various different battery chemistries, redrawn from ref[4]. B) Schematic illustration of the Li-ion movement in a rocking chair type of battery such as a Li-ion battery.

Fig. 2 depicts a battery in operation. Apart from the anode and cathode, the electrolyte and separator are of crucial importance for its functionality. The basic function of the electrolyte is to be electronically insulating while at the same time being ion-conductive. This provides a path for the ions to move, while forcing the electrons out in an external circuit, thus achieving the separation in space of the required oxidation and reduction. While electrodes and electrolytes are the battery parts of conceptual importance, there are also some ever-present materials of functional importance presented in Fig. 2. The separator, for example, is a physical barrier used to prevent contact between the anode and cathode and thus short-circuiting the battery. The separator is soaked in electrolyte and needs to be porous to allow the electrolyte to provide ionic conduction between the electrodes. Moreover, the electrode materials are cast on metal foils that provide electronic connection to the external circuit; these metal sheets are most often referred to as current collectors.

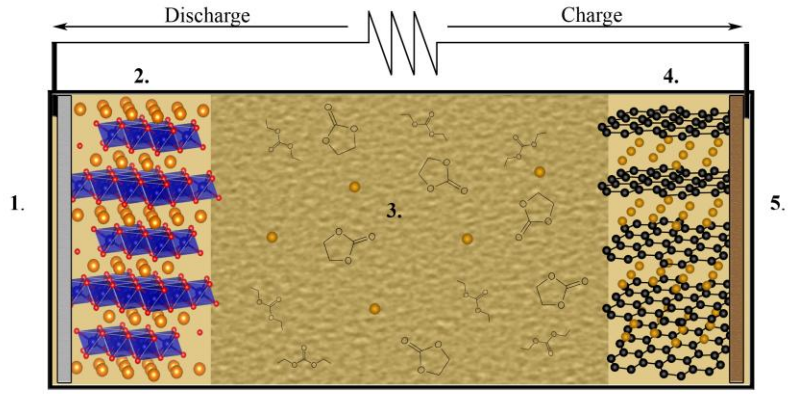

Figure 2. Schematic representation of a battery in operation displaying all vital components for functionality; 1: Cathode current collector, typically aluminum. 2: Cathode composite electrode. 3: Polymer separator soaked in electrolyte. 4: Anode composite electrode. 5: Anode current collector, typically copper.

1.2 Electrode materials

1.2.1 Cathode materials

The cathode serves as a lithium host, accepting lithium ions generated from the anode and transported through the electrolyte during discharge. The cathode material needs to be stable, but not so stable as to render the lithium acceptance process irreversible as in primary batteries. Good materials for this purpose proved to be intercalation materials, i.e. materials in which lithium ions could position themselves in vacancies within the structure without significantly changing the overall structural properties. The intercalation process can easily be reversed by applying a reversed voltage of almost the same magnitude as at which the intercalation took place.

In the first commercialized battery from Sony in 1991, lithium cobalt oxide ($LiCoO_2$, LCO) was the cathode material of choice. Displaying reasonable performance and price, LCO was the best candidate of the time, but drawbacks such as high cost and toxicity of Co and generation of O_2 at overcharging urged further research into new cathode materials[5–7]. Sub-families to LCO, utilizing addition of other metals such as manganese, nickel, and aluminum to form materials such as lithium manganese cobalt oxide (NMC) or lithium nickel cobalt aluminum oxide (NCA) improved the thermal stability of these layered oxides and have shown promise for new cathode materials, although the problem with the presence of Co still remains. Investigations of iron based cathode materials have been conducted, since Fe is an

earth abundant metal that would allow for low-cost production, and during these studies lithium iron phosphate ($LiFePO_4$, LFP) was found to fulfill many requirements. Being a very robust system with moderate potential, LFP has developed into one of the dominant materials in commercial LIBs.

Quite early in the LIB development, lithium manganese oxide spinel ($LiMn_2O_4$, LMO) was explored as a potential cathode material, but the intrinsic problem with manganese dissolution proved difficult to overcome. The dissolution problem was argued to be due to that the average oxidation state of manganese (+3.5) was unstable, and manganese thus tends to disproportionate into the +II and +IV oxidation states ($Mn^{+III} \rightarrow Mn^{+II} + Mn^{+IV}$) [8,9]. When trying to solve the dissolution problem, a LMO derivative was found in lithium manganese nickel oxide ($LiMn_{1.5}Ni_{0.5}O_2$, LMNO), which showed very interesting properties in terms of an increased intercalation potential from ~4 V to ~4.7 V as compared to the LMO material, making LMNO one of the early high voltage cathode materials[10]. The extra voltage would allow the battery to perform more work, making it worthwhile to try to find electrolytes compatible with the extended voltage stability window necessary.

1.2.2 Anode materials

In the early stages of development, pure lithium metal was used as anode in batteries, but this proved hazardous. During recharging of the battery, the lithium ions always move the shortest route from the cathode to the anode. This means that any topographical irregularity becomes enhanced building over time and dendrites start to grow. The dendrites will eventually grow over to the cathode, thereby shorting the battery and in the worst case scenario causing a thermal runaway leading to a fire or small explosion. To circumvent this safety hazard, researchers explored other solutions. Three families of alternative materials have primarily been investigated: intercalation, conversion and alloying materials[1,11].

1.2.2.1 Intercalation materials

The working principle of intercalation is to position lithium-ions within a host matrix in the interstitial vacancies of the parent material. No general structural change occurs and no covalent bonds are broken or formed which affords a comparatively easy insertion/deinsertion of lithium-ions into the structure. Graphite was the first anode intercalation material to be commercialized by Sony in 1991. With an intercalation material as the anode, the risk of dendrite formation was greatly reduced. Graphite intercalation occurs at 0.125 V vs Li^+/Li (all potentials will hereafter be referred to Li^+/Li unless otherwise stated) resulting in a very small potential loss as compared to lithium metal. Lithium titanate ($Li_4Ti_5O_{12}$, LTO) with a potential of 1.55 V has been suggested as a new anode material[12–15], but the gravimetric capacity of

175 mAh/g for LTO is low compared to the 372 mAh/g of graphite, and the availability and price of graphite is much more appealing than for LTO, thus causing graphite to remain as the dominant choice as anode in modern LIBs. The relatively low lithium to material ratio in intercalation materials unfortunately results in a low gravimetric capacity compared to the alternatives discussed below.

1.2.2.2 Alloying materials

Elements that form alloys with lithium are the second family of materials investigated as possible alternatives for use as anodes[11]. Alloying materials present significantly higher gravimetric capacities as compared to graphite. Among the studied elements of choice, tin, silicon, aluminum and magnesium can be found. Silicon is perhaps the most thoroughly studied element due to its abundance and capacity to store 3600 mAh/g as compared to 372 mAh/g for graphite. Alloying materials, however, have other intrinsic problems. The chemical changes during battery operation cause a large volume change of the material, which is around 300 % in the case of silicon. This large volume change has proven to cause problems with the structural integrity of the battery; the electronic contact is lost due to mechanical fatigue. Also due to the large volume changes, the passivation of the electrode will not be complete, leading to continuous electrolyte degradation. This issue is more thoroughly discussed in the section on the electrode/electrolyte interface.

1.2.2.3 Conversion materials

Conversion materials function through an exchange reaction as expressed in equation 1[11]:

$$M_xN + yLi^+ + ye^- \leftrightarrow xM + Li_yN \quad (1)$$

where M is a transition metal (Fe, Co, Mn, etc) and N is an electronegative element (O, S, P, etc). Iron oxides and other metal oxides have been the target of much research. A high theoretical capacity and low cost make them favorable options. Analogous to the alloying materials, however, the conversion materials also suffer from large volume changes and electrolyte decomposition. Additionally, many conversion materials have the slowest kinetics of all three types of anode materials which this gives rise to a rather large voltage hysteresis in batteries built using these materials, which in turn corresponds to a low battery efficiency (i.e. large losses).

1.3 Electrolyte

The essential function of the electrolyte is to facilitate lithium ion conduction between the electrodes. The requirements on the electrolyte are then that the electrolyte is ionically conductive, electronically insulating, and chemically inert with respect to all other constituents of the battery. There exist many different types of electrolyte which can be categorized into different families depending on their material properties: liquids, solid polymers, ceramics, gels, and ionic liquids[16]. Among these, the liquid electrolytes are the ones dominating the commercial market by being the only candidate with high enough ion conductivity to meet the performance requirement in many applications of LIBs.

The operation potential of a battery usually spans several volts, and the electrochemical stability window (ESW) of water of around 1.2 V is far too narrow to allow water to be suitable as a LIB electrolyte solvent. Therefore, liquid electrolytes generally consist of a lithium salt dissolved in an organic solvent. Apart from a wide ESW, a good solvent should also have a high dielectric constant, low viscosity, and melting- and boiling points within an appropriate interval. No single solvent has so far provided all these properties and the electrolyte is therefore generally a mixture of solvents. Ethylene carbonate (EC) and diethyl carbonate (DEC) in a 1:1 ratio is a common combination today. EC is sensitive to reduction at the anode, decomposing by forming a thin film that passivates the graphite electrode. Apart from the film-formation, EC provides a high dielectric constant that favors dissociation of the lithium salt which is needed for high ion conductivity. The drawback of EC is its high viscosity and melting point (~36 °C), and to counter this DEC is added.

The first lithium salt used in a commercial battery was lithium hexafluorophosphate ($LiPF_6$). While not optimal in terms of thermal stability or sensitivity to moisture, $LiPF_6$ is important for protection against corrosion of the aluminum current collector on the cathode side. The passivation of the aluminum occurs by forming a protecting aluminum (oxy-)fluoride layer by accepting fluorine from the salt anion. Proposed replacements of $LiPF_6$ can primarily be divided into three groups: $LiPF_6$ derivatives, imide-based salts, and chelating borate-based lithium salts. The derivatives try to mimic the fluorine donating properties of $LiPF_6$ while improving the stability. The imide salts improve battery safety and salt stability considerably, but fail to passivate the aluminum. Finally, the chelating borate-based salts are more environmentally friendly and possess passivating properties, but have lower ion conductivities due to large and bulky anions.

1.4 The electrode/electrolyte interphase

The electrochemical stability window (ESW) of the electrolyte solvent determines if the latter will be stable over the entire operating voltage window of the battery. The HOMO/LUMO gap of the solvent is therefore a decisive factor. If the operating potential of the electrode is not within the ESW of the electrolyte, electron transfer can occur between the electrode and the electrolyte as depicted in Fig. 3a. In the standard graphite/LCO cell, LCO is within the ESW of most common electrolytes while graphite is not. The onset of electrolyte reduction starts around 0.8-1V in common electrolyte solutions, thereby making the graphite electrode a site for electrolyte reduction. The widespread implementation of graphite in LiBs is still possible by the formation of what is known as the Solid Electrolyte Interphase (SEI) layer. When electrons are injected to the LUMO of the electrolyte and thereby reducing it, the reduction products accumulate on the surface of graphite and form the SEI. The SEI is ionically conducting while electronically passivating. This prevents electrons from graphite to react further with the electrolyte, while still allowing battery operation since ions can move through the SEI layer. As shown in Fig. 3b, the formation of the SEI passivates the surface of graphite and prevents further decomposition by limiting electron transfer. Other effects of the SEI are an increased internal resistance and a loss of lithium-ions, which is why an overly abundant formation of SEI would deplete the battery of salt or render it useless due to high internal resistance. Therefore, additives in the electrolyte such as vinylene carbonate (VC) or fluorinated ethylene carbonate (FEC) have been employed to modify and control the formation of the SEI to generate a fine continuous film that passivates completely but do not add too much internal resistance. The implementation of a high voltage anode such as LTO should impact the SEI formation dramatically since the operation potential of 1.55 V is well within the electrolyte ESW, as depicted in Fig. 3c. Utilizing a high voltage anode would also allow usage of electrolyte solvents that are not stable with graphite, but which would possess beneficial properties such as lower melting points or higher ionic conductivities.

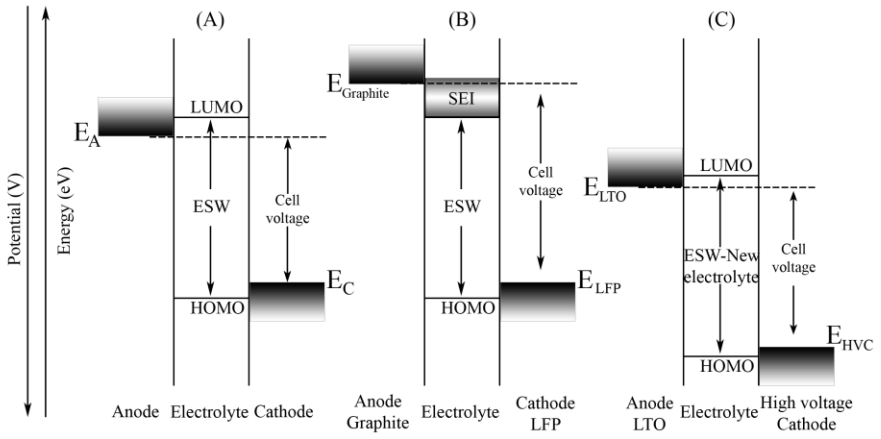

Figure 3. A schematic illustration of potentials leading to SEI formation in batteries. (A) Display the ideal case where the potential of the anode (E_A) and the potential of the cathode (E_C) are within the electrochemical stability window of the electrolyte. In (B), the practical situation of an LFP|graphite cell is shown. The potential of LFP is within the ESW whereas the potential of graphite is not, leading to the formation of an SEI layer that passivates the graphite surface. (C) Illustrates a possible solution for a battery comprising LTO and a high-voltage cathode using a new electrolyte system.

2. Lithium titanate as an anode material

The low electrochemical potential associated with lithium intercalation in graphite poses a risk in certain circumstances; the problem with lithium dendrites is not completely avoided, and under cold conditions or at high current densities, lithium plating and dendrite formation can occur on the graphite surface. In this context, LTO was suggested as a replacement for graphite in high power applications since the working potential of 1.55 V reduces the risk of dendrite formation as compared to graphite. Additionally, the lithiated and delithiated states of LTO possess the same cell parameters, resulting in zero volume change during cycling, thereby making it a zero strain material. Graphite undergoes a 10% volume change during cycling which causes the SEI to crack and enables further electrolyte decomposition. This is regarded as one of the long-term degradation mechanisms in batteries with graphite anodes [17–20]. The zero volume change of LTO would allow for extended cycling without mechanical failure or cracking of the SEI. The choice of LTO as a replacement LIB anode is also considered due to the relative abundance of the required elements, enabling large-scale productions at low costs. However, despite its comparatively high operating voltage, it is not yet fully experimentally verified that LTO is an SEI-free material. The work done in this area[21–29] is not conclusive, and theories in literature encompass the possible presence of an SEI, that the observed changes are due to oxidation products originating from the cathode, and a complete absence of any SEI layer.

The increased safety resulting from the higher intercalation potential of LTO comes with a ca. 1.4 V loss in the cell potential as compared to graphite, with an associated loss in the energy density. One strategy to mitigate this would be the implementation of high voltage cathodes to regain at least some of the lost cell potential, provided that a suitable electrolyte can be found. One suggested cathode material for this task is lithium manganese oxide (LMO, $LiMn_2O_4$) and derivatives thereof, e.g. lithium manganese nickel oxide (LMNO, $LiMn_{1.5}Ni_{0.5}O_4$) or lithium nickel manganese cobalt oxide (NMC, $Li(Ni,Mn,Co)O_2$). The abundance and low toxicity of manganese make manganese spinel materials good candidates for large-scale applications. However, a well-known problem with these materials is the transition metal dissolution into the electrolyte [30]. The dissolution is proposed to be accelerated by the presence of the common lithium salt LiPF6 through a

three-step process involving hydrofluoric acid formation and a following attack on the cathode material [8,9]. Batteries containing spinels or their derivatives experience a cell degradation that is faster than what could be expected from half-cell data, which has led to theories of so-called 'cross-talk' between the electrodes. The effect that these transition metals has on the anode is still a topic of research. Most studied is the effect of manganese on graphite[31–42], involving three proposed interaction mechanisms: reduction to metallic manganese, which poisons the SEI so that it no longer passivates the electrode; ionic complexes of manganese that adhere to the surface of the electrode blocking the ion diffusion path; and a two-step mechanism trying to combine inconclusive data by suggesting a electrochemical reduction to metallic manganese followed by chemical oxidation to a higher manganese valency-state but with enough metallic manganese left to poison the SEI, although below the detection-limit of the analysis methods used.

2.1 Scope of this thesis

The work presented in this thesis is part of a larger project aiming to study the degradation mechanisms in batteries. The exact degradation mechanism is unique for each cell chemistry, and there is therfore much work to be done in the field. This PhD project focuses on heavy hybrid vehicle applications and therefore on cell chemistries which are optimized for power performance and prolonged cycle life, which is why lithium titanate oxide versus lithium manganese spinel has been chosen. As stated above, LTO is intrinsically safe compared to graphite due to its higher intercalation potential, and both the abundance of titanium and manganese as well as their toxicity make this combination a good option for large scale applications.

This thesis describes the surface chemistry of the titanate anode. LTO has been suggested as an 'interphase-free' material, and paper I in this thesis comprises an experimental study aiming to verify or disprove this hypothesis. In paper II, the interaction of the titanate anode with dissolved manganese ions in the electrolyte – whose presence is due to dissolution from the coupled cathode of manganese spinel – is investigated.

For these analyses, the highly surface sensitive technique of photoelectron spectroscopy has been employed as the main characterization method. Complementary measurements of the near edge X-ray absorption fine structure (NEXAFS) were also conducted to get a better understanding of the chemical environment of the manganese on the anode.

3. Methods

3.1 Battery preparation

All cells investigated in this thesis were of the pouch-cell type, where electrodes, electrolyte and separator are hermetically sealed in polymer-coated aluminum bags. Alternatives such as Swagelok-cells would enable studies of pure electrode materials, while coin-cells generally mimic the commercial cells better regarding a low electrolyte content and by avoiding the vacuum sealing, but pouch-cells were nevertheless chosen based on their ease of disassembly for post-mortem analysis.

3.2 Electrode preparation

The electronic conductivity and structural integrity of LTO does not allow usage of the active material in its pure form, and all electrodes used in this thesis were therefore of the composite type. The composite was prepared in three steps. First a slurry consisting of micron-sized $Li_4Ti_5O_{12}$ powder (~9 μm, Life Power® LTO • Phostech Lithium), carbon black powder (Super-P, Erachem Comilog) and Kynar 2801® (Handlapp, dissolved in a 5:95 wt% ratio in N-methyl-2-pyrrolidone) was mixed in a 75:10:15 (LTO:CB:PVdF) weight ratio. Second, the slurry was ball-milled for two hours and then cast on a carbon-primed aluminum/or copper-foil current collector and pre-dried for 10 minutes at 120 °C. Third, electrodes with a diameter of 20 mm were punched out of the foil and moved into an argon-filled glovebox (H_2O<5 ppm, O_2<1 ppm). The electrodes were then dried in a vacuum furnace for 12 hours at 120 °C to remove residual water. Average mass loadings were around 10-30 mg. LMO electrodes were prepared in the same way, but substituting LTO with $LiMn_2O_4$.

3.3 Cell assembly

In Paper **I,** lithium metal was used as counter electrode. In Paper **II,** LTO and LMO electrodes were matched to prepare batteries with 10 % overcapacity in the cathode with respect to the anode. All assembly took place in an air-free environment. The polymer separator (Solupor®), with a diameter of

22 mm and a thickness of 20 μm, was soaked with 75 μl of an electrolyte consisting of 1 M $LiPF_6$ (BASF) dissolved in ethylene carbonate (EC, BASF) and diethyl carbonate (DEC, BASF) in a 1:1 volume ratio. The cell stack was vacuum-sealed in polyethylene-coated aluminum pouches, with aluminum current collectors.

3.4 Electrochemical cycling

For the electrochemical testing of the fabricated cells, galvanostatic cycling was used. In this type of measurement a constant current is applied by the galvanostat and the voltage response is measured. In this thesis an Arbin BT-2043 and a Digatron BTS-600 battery testing systems were used to cycle the cells. This is a widely employed technique for long-term battery testing. Often the rate at which the cells are cycled is referred to as the C-rate. C denotes 100% of the capacity and by convention the C-rate is expressed in terms of the number of hours over which the capacity is depleted, i.e. C/10 would be one full discharge in ten hours; a complete cycle would then take twenty hours. Fractions of hours, for example one half hour, would then correspond to be C/0.5, which is written as 2C.

3.5 Analysis preparation

The SEI of the electrodes is extremely sensitive to air, and therefore all analysis preparations were done in a argon-filled glovebox. Cells were dismantled, the electrodes were cut into pieces suitable for measurement and then washed with dimethyl carbonate (DMC) thoroughly to remove any unwanted residues before mounting them onto a sample plate. The samples were transferred from the glovebox to the analysis chamber using a home-made airtight magnetic rod to prevent any exposure to air.

3.6 Characterization techniques

3.6.1 Photoelectron Spectroscopy

In 1905, Albert Einstein published his theory of the photoelectric effect, built upon ideas of Max Planck[43]. Revolutionary for his time, Einstein suggested a theory where light was not treated as a continuous wave, but as discrete quanta of energy, today known as photons. The photoelectric effect stated that certain materials would emit electrons when absorbing photons with a certain energy. In the mid-1960s, Kai Siegbahn worked out a method to use

this for chemical analysis; a method then coined Electron Spectroscopy for Chemical Analysis, ESCA, but which today is more widely known as Photoelectron Spectroscopy, PES, or X-ray Photoelectron Spectroscopy (XPS). The working principle of PES is to irradiate a sample with monochromatic photons and then measure the outgoing intensity of the electrons as a function of the photon energy[44]. According to orbital theory, electrons occupy distinct energy levels, unique for each orbital and element. If both the energy of the photons and ejected electrons are well defined, the ground principle for determining the binding electron energy from PES can be expressed as:

$$KE = h\upsilon - BE - \phi_s \quad (2)$$

Here, KE is the kinetic energy of the outgoing electron, $h\upsilon$ the ingoing energy of the photon, BE the binding energy of the orbital of the electron, and ϕ_s is the work function of the spectrometer used. The unique orbital levels of each element make PES an element sensitive technique, enabling identification of all of the different atoms in the measured sample. Chemical bonds will degenerate the orbitals, giving them a slightly altered energy and thereby resulting in so called chemical shifts. Since the chemical shifts are well defined for each type of bond, PES is also a powerful tool for determining the chemical environment of the analyzed element to give a picture of the chemical surface composition of a sample.

After photoionization, a secondary relaxation process can occur in which an outer shell electron fills the gap left by the photoelectron, in a process where an additional electron from the same shell is sent off carrying the extra energy from the relaxation. This electron is called an Auger electron. The Auger energy is also element specific and some precautions may be needed to avoid interference of the Auger electrons with the PES measurements.

To be able to distinguish between all electrons present in the PES measurement, a hemispherical analyzer from VG Scienta was used in all experiments in this thesis. The analyzer consists of an electron photomultiplier detector and a hemispherical electron filter. The analyzer functions by applying a voltage over the hemisphere, curving the path of all electrons entering so that only electrons with the desired energy will reach the detector. This makes it possible to plot the counts as a function of energy.

The photon interaction with matter usually allows for penetration of the sample to a depth of 1-10 micrometers. However, an electron interaction with matter is much more probable than that of a photon, making the escape depth of electrons in the range of Ångströms in solids and up to nanometers in organic polymers. The escape depth is dependent on the Inelastic Mean Free Path (IMFP, or λ), i.e., the distance traveled in a material without any loss of energy. The probing depth, i.e. the depth actually analyzed is $3\times\lambda$, a depth at which 95% of the recorded signal will originate. The IMFP is de-

pendent on the kinetic energy of the electron, and by varying the incident photon energy in the measurements, depth profiling can be achieved non-destructively. The ability to study the chemical composition together with the high surface sensitivity have made PES one of the most powerful and widely used surface analyzing techniques employed today.

3.6.2 Synchrotron radiation source

A normal PES equipment has a radiation source constructed of a metal filament that generates photons with a specific defined energy. The most common filament materials are magnesium (Mg Kα 1253.6 eV) and aluminum (Al Kα 1486.6 eV). One drawback with these regular sources is that they are static, rendering only one wavelength. This allows only fixed probing depths, and corrections can be problematic in the event of overlapping Auger peaks. Synchrotron radiation sources, on the other hand, exploit the fact that electrons under acceleration emit photons over a wide energy range. The basic principle of the synchrotron is to have a large ring in which electrons are injected, while undulators along the ring generate an oscillating electric field which the electrons pass and therefore emit photons. The photons are monochromated through utilizing mirrored single crystals of silicon that diffract the photons according to Bragg's law.

3.6.3 Near edge X-ray fine structure

The fundamental mechanism of Near Edge X-ray Fluorescence Structure (NEXAFS) is presented in Fig. 4a. As in PES, the excitation process in NEXAFS is caused by a photon exciting an electron in a core level orbital. But in contrast to PES, the photon in a NEXAFS measurement is not used to knock out a photoelectron, but to excite a core level electron to unoccupied orbitals. The energy of the incoming photons varies between an energy that is equivalent to the difference between the core-level and the HOMO level to an energy that is the difference of core-level and vacuum level, see Fig. 4a. This produces excitation to all possible excited states of the atom[45]. This excited state will be terminated by one of three different processes, shown in Fig. 4b. These processes can emit photons or electrons which can be measured, either by a fluorescence detector or by the feedback current to the sample when replacing ejected electrons. A fluorescence detector was used in this thesis work. The energy difference between the core level and the LUMO is dependent on the oxidation state of the atom, thus making NEXAFS able to determine the oxidation state of the element by observing at which energy excitation starts to occur. The fluorescence detector measures photons indiscriminately of origin and the resulting response will therefore be a summation of all possible excited states, which in turn depends on the unoc-

cupied orbitals. The chemical environment of a measured element will result in unique unoccupied molecular orbitals, making the post-edge shape of the resulting wave dependent on the chemical state; see Fig 4c. Therefore, NEXAFS can be used to probe the chemical environment as well as the oxidation-state of an element.

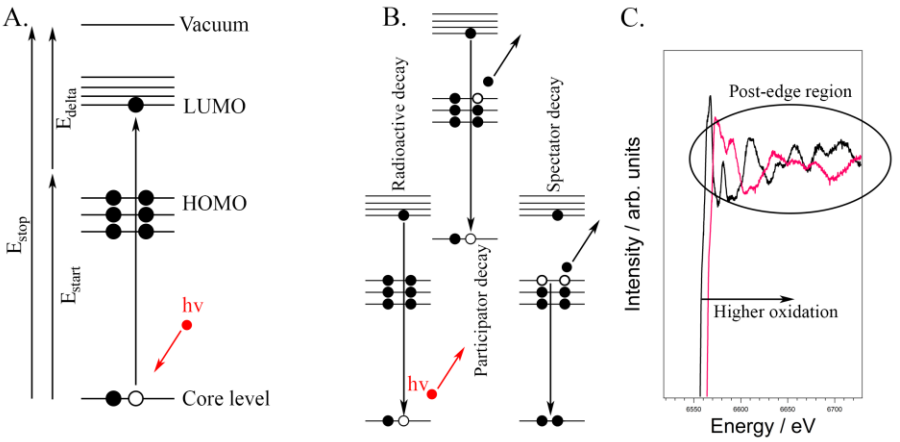

Figure 4. A: The fundamental processes of NEXAFS. B: NEXAFS relaxation processes. C: Example of NEXAFS data.

3.6.4 Data processing

The intensity of the signal in PES is directly proportional to the amount of the element measured and can be described by:

$$I = n \times f \times \sigma \times \theta \times y \times \lambda \times A \times T \qquad (3)$$

In this equation, I is intensity, n is number of atoms of the element per cm^3, f is the flux of photons per cm^2, σ is the photoelectric cross-section of the atomic orbital in cm^2, θ is the angular efficiency of an electron reaching the detector (dependent on the angle between incoming photons and measured electron), y is the efficiency of the photoelectric process, λ the mean free path, A is the area from which photoelectrons are detected, and T is the detection efficiency of the electrons emitted. A quantitative analysis can be done if all factors are known. This is a cumbersome task, but it is fairly straightforward to do a relative intensity comparison between samples in order to observe changes in composition. In a single core level measurement on one sample, all these factors remain unchanged, and therefore the amount of different components in a deconvolution is directly related to the area under the peak of the substance. All spectra were calibrated using the main carbon peak as a reference and assigning this to the C-H bonds at 285 eV. All spectra were also normalized to the highest peak. The NEXAFS spectra

were intensity normalized in a three step process: first the spectra were adjusted to the incoming beam intensity by dividing the fluorescence intensity with the beam intensity; thereafter adjusting for the noise level by subtracting a flat linear background where the background level of the pre-edge served as a level adjuster; and finally the spectra were normalized with the equilibrium level of the tail as the normalization point. All PES data processing has been done in Igor Pro version 6.34A.

4. Results and discussion

4.1 SEI on LTO in half-cells

4.1.1 PES on half-cells

The first part of this thesis work, described in Paper I, was to examine the surface layer of LTO half-cells to establish the possibility of the existence of an SEI layer on LTO, contrary to previous assumptions. A half-cell is a concept in which lithium metal is used as a counter electrode, effectively creating a cell where only one material of interest is present; this is frequently done in battery studies to investigate the properties of one material at a time. In Paper I, LTO half-cells were cycled for 5 and 100 cycles between 1.0-2.0 V and subsequently analyzed with PES.

Reference samples are important in PES analysis; this is in order to be able to determine changes over time, and therefore a pristine electrode and a battery stored at open circuit voltage (OCV) were also studied and compared to the cycled samples.

The survey spectra of the samples are presented in Fig. 5. If LTO constitutes an SEI-free material, the survey spectra of the samples should be identical to that for the pristine electrode. However, clear differences can be observed, as shown in Fig 5. These changes are most likely due to an SEI formation. Titanium is only present in the titanium oxide which is a bulk material of the electrode, and the relative titanium/carbon intensity is decreasing for all samples compared to that for the pristine electrode. This decrease is most likely caused by an SEI formation since this would result in less photoelectrons from the titanium reaching the detector through the SEI. Carbon, on the other hand, is a constituent of the SEI layer and thereby maintains a relatively high signal from the C1s core-level. That there is a difference between the OCV sample and the pristine electrode suggests that there is electrolyte decomposition occurring spontaneously in the battery, and that no electrochemical activity in the cell is needed. The difference between the 5 cycle sample and the OCV sample is somewhat counterintuitive since the 5 cycle sample is more similar to the pristine electrode, suggesting more SEI formation on the OCV sample than on the cycled sample. Both cells were assembled at the same time, both spent two weeks in the assembled state before the measurements, and the 5 cycle cell was cycled just prior to the PES measurement. The same processes should thus have occurred in both

cells until the galvanostatic cycling was performed, suggesting that the SEI formed initially at OCV can be stripped from the electrode during battery cycling.

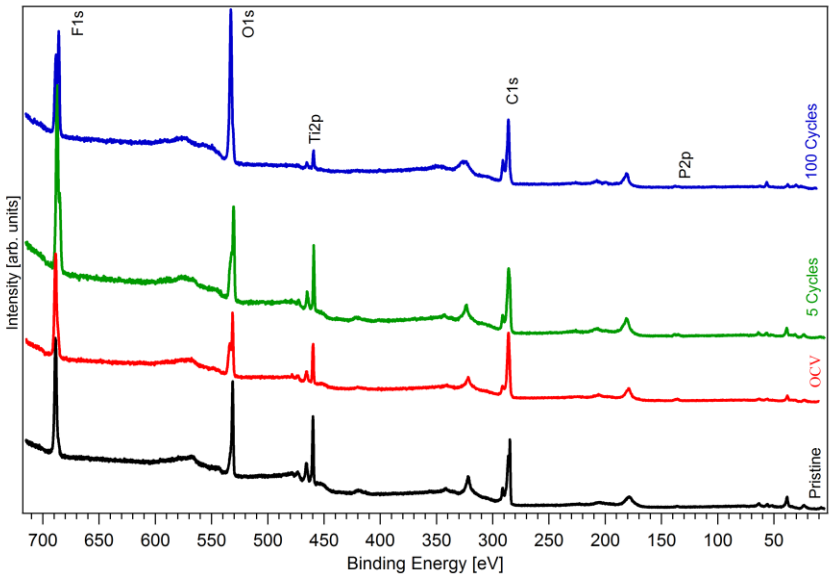

Figure 5. Survey spectra of pristine, OCV, and cycled (5 and 100 cycles) samples. The spectra were normalized with respect to the highest carbon peak.

In Fig. 6, a more detailed analysis of the different core levels is presented. During the measurements, the photon energy was varied so that all outgoing photoelectrons maintained an energy of ~140 eV, thus measuring at a constant depth corresponding to 20-30 Å for all elements [46]. Carbon-carbon bonds in the conductive carbon and carbon hydrogen bonds in the polyvinylidene difluoride (PVdF) binder were assigned to the peaks at 284.4 eV and 286 eV, respectively. The peak at 291 eV was assigned to carbon-fluorine bonds[22]. Carbon species such as O-C-O and C=O were found at the energy of 287.5 eV, while carbonates are at 290.3, and ether bonds were found at 287 eV[47].

The C-C bond of the conductive carbon and the -CF_2- bonds in PVdF originate from the defined repetitive structure in these compounds and will not be altered by or recreated in an SEI formation process. They can therefore be seen as signals only originating from the bulk. When comparing the C1s spectra of the pristine sample with that of the OCV sample, there are some discernable differences. Most prominent is the reduction in the signal from the conductive carbon. There also seems to be an addition of carbonate species and C=O/O-C-O bonds for the OCV sample as compared to the pristine electrode. All in all, this is consistent with the decreasing titanium/carbon ratio in the survey spectra and an indication of the formation of an SEI. Carbonates and C=O/O-C-O groups are both normal components in

an SEI layer on graphite using the same electrolyte system. Since the conductive carbon peak was still visible as a shouldering in the OCV sample, the estimated SEI thickness was between 20-30 Å since the probing depth was 30 Å.

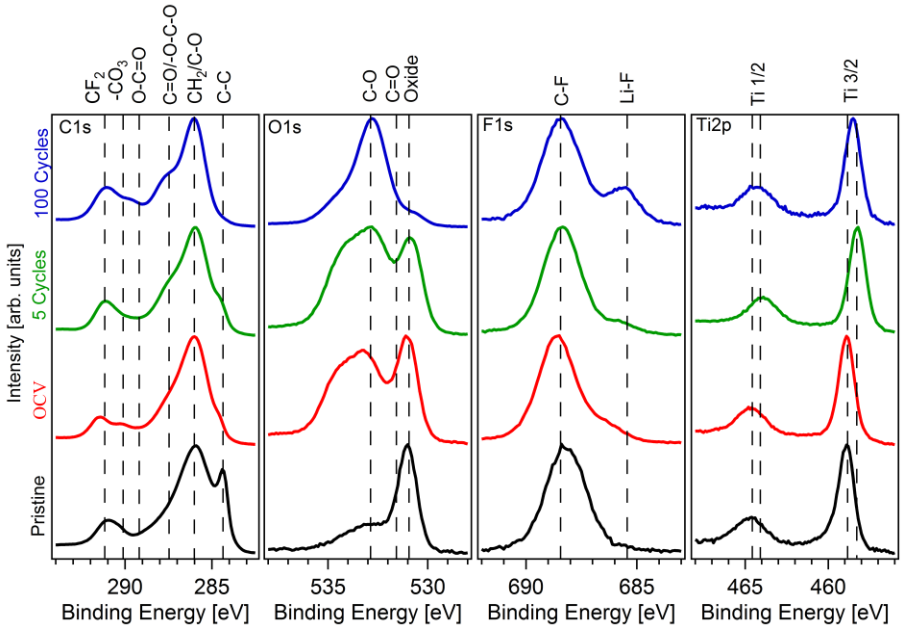

Figure 6. The C1s, O1s, F1s, and Ti2p PES core levels signals of the pristine, OCV, 5 cycles, and 100 cycles samples. The excitation energy was varied to keep a constant energy of 140 eV for the photoelectron.

When analyzing the 5 cycle sample data, there are some notable differences, both with respect to the pristine electrode and to the OCV sample. Compared to the pristine sample the conductive carbon peak intensity was reduced, but compared to the OCV sample the relative amount of conductive carbon peak was slightly increased. This is again in agreement with the decreasing titanium/carbon ratio in the survey spectra, and also with the theory of electrochemical stripping of the spontaneously formed SEI from the electrode. Other notable features are that in the 5 cycle sample, the -CF_2- peak was more prominent than for the OCV sample; i.e., there were less carbonates in the SEI of the 5 cycled sample than in the OCV sample, and there were more ethers in the cycled sample than in the OCV sample. The ratio of C=O/O-C-O to CH_2/C-O was larger for the 5 cycle sample than for the OCV sample. This suggests that not only are the spontaneously formed SEI stripped away during cycling, but the SEI formed during electrochemical cycling has another composition than the one spontaneously formed.

Comparing the 100 cycle sample to the 5 cycle sample, the relative intensities of the O-C=O and C=O/O-C-O peaks increased, i.e. the same peaks

that were the difference between the 5 cycle sample and OCV sample. This indicates that these were the species promoted in the SEI formed during cycling, and present in a different ratio than in the SEI of the OCV sample. The peak of the conductive carbon was completely absent in the spectra of the 100 cycle sample, suggesting that the SEI reached a thickness greater than 30 Å. The 100 cycle samples were assembled at the same time as all the other cells, and while the 5 cycle sample was stored for some time before cycling, the 100 cycle sample started cycling immediately after assembly and was measured directly after the cycling had stopped. In conclusion, the OCV sample had only a spontaneously formed SEI, while the 100 cycle sample primarily had an electrochemically induced SEI. But since only the 100 cycle sample had completely lost the conductive carbon peak, the growth-rate of the SEI appear to be faster for the electrochemically induced SEI, at least for the C-rate investigated.

In the O1s spectra in Fig. 6, the peak at 531 eV was ascribed to the O^{-II} in the LTO particles[29]. The C-O bonds were assigned to 533.5 eV, C=O at 532.2 eV, and the peak at 534.8 eV to $Li_xPF_yO_z$. $Li_xPF_yO_z$ is a general expression for all different products of $LiPF_6$ salt degradation, which is known to include hydrofluoric acid generation, in turn yielding lithium fluoride[48]. In the pristine sample, only the bulk oxygen signal is visible together with a small amount of oxygen contaminations. The O1s spectra of the OCV sample show that compared to the pristine sample, new species were present on the surface. These new species mostly consist of C-O single bonds, but signals from salt decomposition products and C=O double bonds were also present. The C=O bond is much more prominent, and the C=O/C-O ratio is greater for the 5 cycle sample than for the OCV sample. The ratio between the peak areas of the C/O species and bulk oxygen increased for the OCV sample compared to the cycled LTO, indicating more SEI formation on cycled LTO particles than on LTO particles stored at OCV conditions. Putting these result in context of the C1s spectra where the OCV sample generally shows more C/O products, this implies that the spontaneous degradation is preferential to carbon additives in the electrode while the SEI formed during cycling are uniform over the electrode. The bulk oxygen peak was almost completely gone for the 100 cycle sample, and the C=O/C-O ratio was even higher than for the 5 cycle sample, indicating more SEI formation after 100 cycles. Moreover, C=O species were formed to a higher degree than other compounds. The contributions from salt degradation products were lower for the 100 cycles sample when compared to the 5 cycle sample, indicating that the salt decomposition is more prominent in the early phases of the continuous electrolyte decomposition process.

In the F1s spectra, the C-F bond from PVdF at 688.5 eV and the Li-F peak at 685.5 eV can be observed. No large differences exist between the spectra for the OCV and pristine electrodes, although the signal from Li-F

was growing with increasing cycle number indicating an electrochemically driven decomposition of the salt.

There have been some studies carried out to investigate how the SEI layer would affect a photoelectron originating from the bulk. Clark et al. made studies on a gold plate onto which a polymer film had been deposited and found a peak shift depending on film thickness[49]; shifts of up to two eVs for films of up to 80 Å were observed. This could account for the shift observed between the cycled samples and the OCV and pristine samples in the Ti2p spectra in Fig. 6.

Moreover, Fig. 7 presents more conclusive evidence for the presence of an SEI. The only source of phosphorus in the cells was the lithium salt anion in the electrolyte. In the P2p spectra, the peak at 135 eV is assigned to P-O bonds while the peak at 138 eV corresponds to the PF_6 group in the salt. The pristine sample is not presented since there was no response from phosphorus for this sample. In Fig.7 an increase in electrolyte decomposition can be observed from 5 cycles to 100 cycles but most electrolyte degradation products compared to trapped PF_6 are found in the OCV spectra. The presence of phosphorus confirms SEI formation in all three samples.

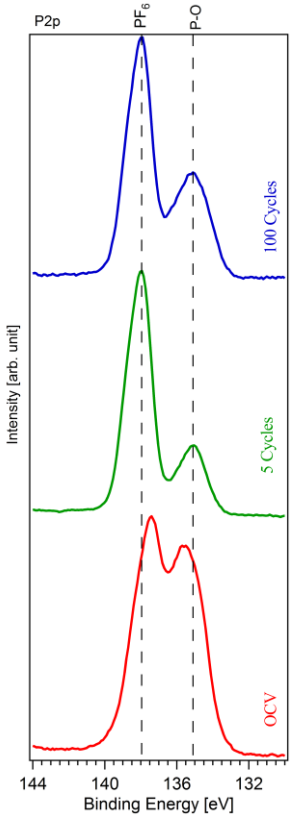

Figure 7. P2p core level PES signals for OCV sample, 5 cycle sample, and 100 cycle sample.

4.1.2 Depth profiling

By using different excitation energies in PES, a non-destructive depth profiling can be obtained. An increase in the excitation energy results in a larger kinetic energy of the photoelectron, and the higher energy of the photoelectron results in a longer IMFP and thus a larger probing depth. Presented in Fig. 8 are the different core-levels of the 100 cycle sample for two different energies, one with a calculated kinetic energy of the photoelectron of 140 eV (blue) and one with excitation energy of 835 eV (black), where the latter hence provided a deeper probing.

The C1s spectrum of the larger probing depth shows the bulk peak of the conductive carbon, in contrast to the total absence of this peak in the surface spectrum. This trend is also visible for oxygen where the ratio O^{-II}/C=O increased with larger probing depth. An excitation energy of 835 eV would be equivalent to a probing depth of 50-60 Å, indicating that the SEI was thinner than this but thicker than 30 Å which would block the signal from 430 eV excitation energy. This renders an estimated thickness of the SEI of 40-50 Å.

Most notable in Fig. 8 is the large difference between the two P2p spectra. The contribution of the salt decomposition product P-O was a lot larger with higher excitation energy, implying that there was a higher concentration of salt decomposition products deeper in the SEI. This can be related to the O1s spectra in Fig. 6, which show the same trend. For the 5 cycle sample, there was a larger contribution from $Li_xPF_yO_z$ than for the 100 cycle sample, implying that salt decomposition products constituted a larger part of the SEI during the early stages of the SEI formation.

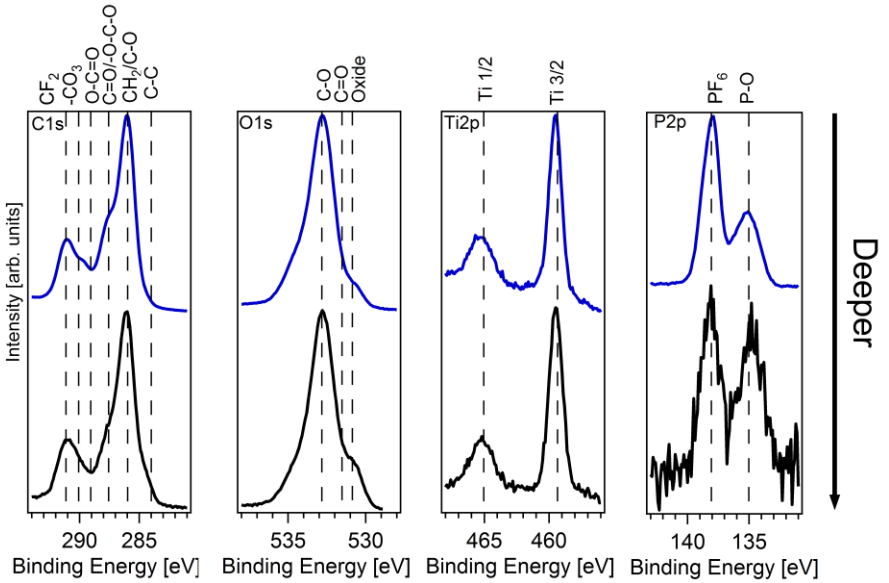

Figure 8. C1s, O1s, P2p, and Ti2p PES spectra of a sample cycled for 100 cycles using different excitation energies yielding different depths of analysis.

4.1.3 Potential windows

In Fig. 9, PES data of the 100 cycle sample are presented together with the PES data of a reference cell of the same composition but cycled under different conditions: 100 cycles in the voltage window of 1.4-2.0 V instead of 1.0-2.0 V. The onset of electrolyte reduction is expected to start at ca. 1 V, and a cycling window at 1.4-2.0V would then be less likely to incur SEI formation. The main difference between the two samples is observed in the P2p spectra which display a higher relative concentration of P-O bonds for the narrower voltage window. This is in accordance with the O1s spectra which show a higher O-F/C-O ratio for the sample cycled between 1.4-2.0 V. The sample cycled between 1.4-2.0 V is expected to yield less degradation products, and the observation that relatively more salt degrades for this sample implies that the salt is more prone to decompose than the solvent. The spectra for the sample cycled in the 1.4-2.0 V range were also more similar to those for the OCV sample than those for the 1.0-2.0 V cycled sample. This indicates that the electrochemical stripping of a spontaneous formed SEI is dependent on voltage.

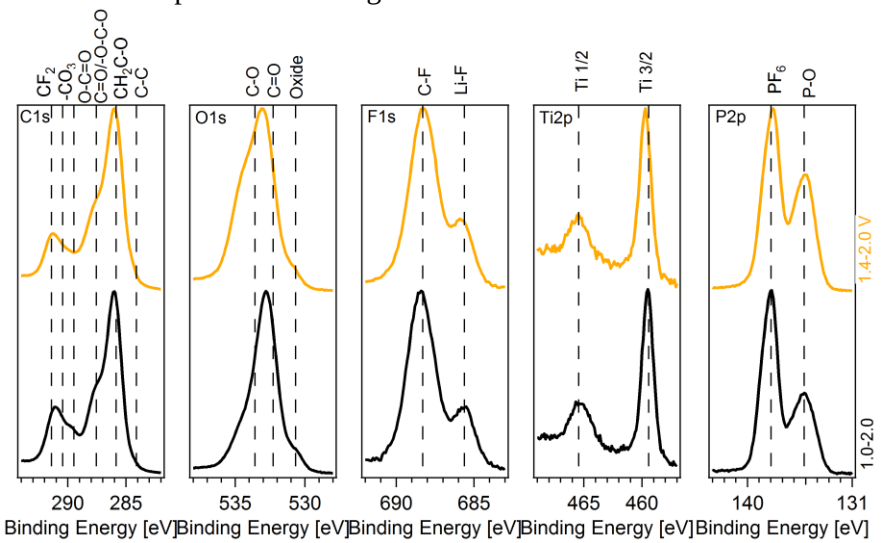

Figure 9. C1s, O1s, F1s, P2p, and Ti2p spectra of samples cycled 100 cycles in voltage windows of 1.0-2.0 V and 1.4-2.0 V, measured with calculated kinetic energies of 140 eV.

4.1.4 Implications from half-cell investigations

In conclusion, all PES data give indications that there was indeed an SEI-layer present on the LTO electrode. The main components of this layer can be characterized to be O-C=O, C=O/O-C-O, and $-CO_3$ containing compounds (i.e, ethers, esters, ketones and carbonates) and salt decomposition products. The most sensitive part of the chosen electrolyte seems to be the

salt, which is the easiest and therefore the first component to decompose. In Fig. 6 the conductive carbon peak is almost gone for the OCV sample whereas the bulk O^{-II} is clearly seen. This can be compared to the cycled samples for which both the C and O bulk peaks disappear with increasing cycle number. This indicates that primarily the surface of the carbon additives in the composite electrodes are the catalytic sites for the spontaneous SEI formation. A preference for the conductive carbon species to cause the electrochemically induced SEI formation cannot be ruled out either, since the conductive carbon peak was completely gone after 100 cycles while O^{-II} was still visible.

4.2 Full-cell investigations

4.2.1 PES on full-cells electrodes

After establishing the existence of an SEI on LTO electrodes, the second part of this thesis (Paper II) investigates this layer in a full-cell, as well as to determine if/how manganese ions could influence the SEI. As described in more detail in Paper II, the cells tested were LTO||LMO cells with 10% overcapacity on the LMO electrode, 1 M $LiPF_6$ in EC:DC 1:1 electrolyte, cycled for 30 cycles. At the end of cycling, one of these cells was charged so that LTO became lithiated while another was left in its delithiated state. The PES measurements done on the full-cells were conducted using higher photon energies, this is because the facility at which the measurements were performed could not go as low in photon energy as the previously used facility, but could instead offer the possibility to measure NEXAFS on the same sample without moving it. As in the half-cell study, an OCV sample and a pristine electrode were studied as references.

In Fig. 10, the PES data for LTO electrodes used in the full-cells are presented. For the C1s core level, the peak assignment of C-C was to 285 eV, -CH_2-CH_2- to 287 eV, O-C-O/C=O to 286 eV and –CF2 bonds to 291.5 eV. In the O1s spectra, O^{-II} oxide was assigned to 531.2 eV, C=O to 532.8 eV, and C-O to 534.1 eV. Comparing the OCV sample with the pristine electrode, indications of spontaneous SEI formation can be observed for the full-cell, in agreement with the half-cell data. The changes were less prominent in the full-cell data due to the higher excitation energy of 2005 eV, with the result that the majority of photoelectrons will be originating from the bulk of the electrode. For the OCV sample, an increase in the signal from C-O compared to the pristine sample can be observed. The peak due to -CF_2- seems to shift to a slightly lower energy which could be the result of the presence of nearby –CO_3 groups. The corresponding increase of C=O and C-O bonds can be observed in the O1s spectra. The formation of an SEI is again confirmed by the P2p spectra, where signals due to incorporated phosphorus-

containing products were found. Similar changes as observed in the OCV sample can also be seen for the cycled samples but less prominent, indicating that a thinner SEI layer was present on the cycled sample than the OCV sample, once again in agreement with the half-cell data and indicating the possibility of a spontaneously formed SEI that is stripped away by electrochemical activity.

The obvious differences between the lithiated and delithiated samples are of particular interest. For the lithiated sample, C-O was increased in both the C1s spectra as well as the O1s spectra, and the general hydrocarbon peak was increased as compared to the delithiated sample. A similar behavior was observed by Song et al. in carbon-free LTO half-cells and this was attributed to adsorption/desorption of SEI/electrolyte decomposition species during cycling[29]. The formed SEI must have been thinner than 20 nm for the bulk O^{-II} to be visible, and the relative intensity of this peak suggest that the thickness was less than this by a good margin.

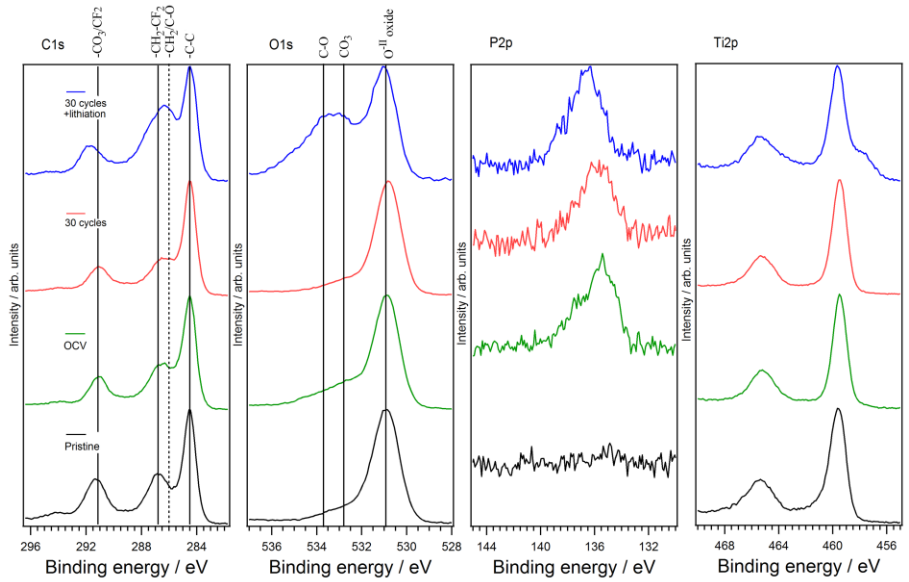

Figure 10. HAXPES spectra depicting the C1s, O1s, P2p, and Ti2p core-levels of the four LTO samples: Pristine, OCV, delithiated and lithiated (after 30 cycles), acquired with a photon excitation energy of 2005 eV.

In analogy to the depth profiling in the half-cell study, the excitation energy was increased for the full-cell measurements as well, and the corresponding data are presented in Fig. 11. The main conclusion from this depth profiling is that all peaks assigned to SEI components had relatively small contribu-

tions to signals at higher energies, confirming that the compounds from which the signals originate were confined to the surface.

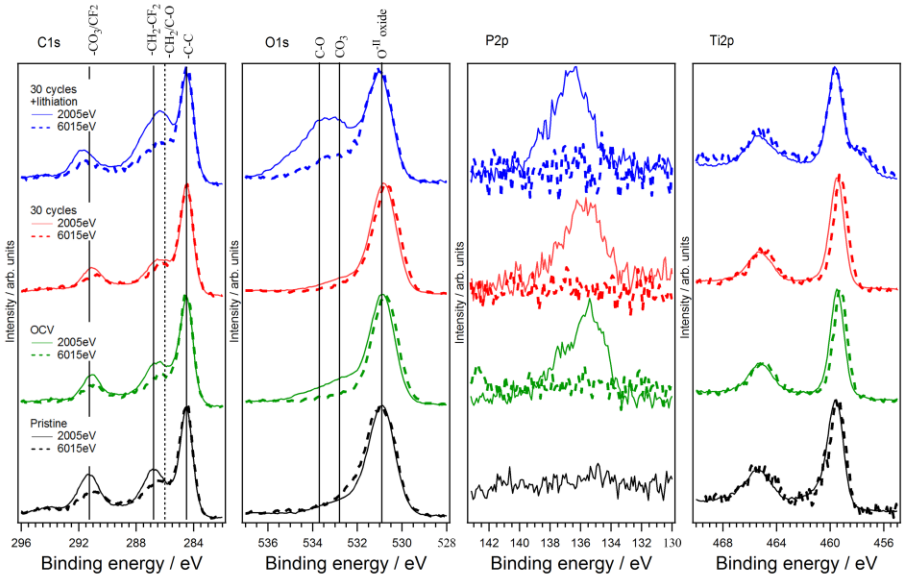

Figure 11. HAXPES spectra depicting the C1s, O1s, P2p, and Ti2p core-levels of the four LTO samples: Pristine, OCV, delithiated and lithiated (after 30 cycles), acquired with photon excitation energies of 2005 eV and 6015 eV.

In Fig. 12, the Mn2p spectra of the four samples are presented, and it can be observed that there was manganese present on all samples except the pristine electrode. There is thus Mn dissolution from the cathode and migration to the anode side in the cell. According to the PES data, the manganese is in its ionic state, but the exact valence state cannot be established from the 2p orbital. It has been stated that the dissolution of manganese is independent of the electrochemical activity [50], while according to Zhan et al. the deposition onto LTO is dependent on cell operation[36]. The present results suggest that the deposition is indeed independent of cycling of the cell.

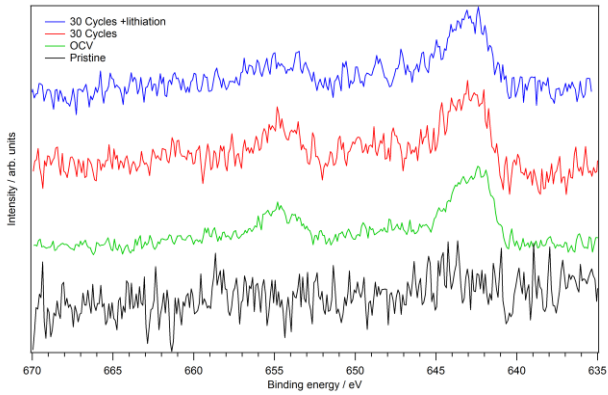

Figure 12. Mn2p core-level spectra of the four LTO samples: Pristine, OCV, delithiated and lithiated (after 30 cycles), acquired with a photon excitation energy of 2005 eV.

4.2.2 NEXAFS

To provide a more complete picture of the manganese species, NEXAFS measurements were performed on the samples. First, to confirm the oxidation-state of the manganese, the NEXAFS absorption edge was compared to the absorption edge of manganese for its known oxidation sates. The absorption edge data are presented in Fig. 12 A. As is clearly seen, the oxidation state of the manganese found in the SEI was between +II and +III, in agreement with the PES data. Theories have been presented that suggest manganese species containing fluoride, oxide, or carbonate in the SEI[34,36,40,42], and reference spectra of these compounds were therefore obtained. The spectra of the delithiated sample and the data for the reference compounds are presented in Fig. 12 B. It can be observed that none of the provided references provided a complete match with the sample spectra, and neither could a good fit be modelled based on the reference spectra. This indicates that the chemical environment of manganese in the SEI layer may not be as simple as previously thought.

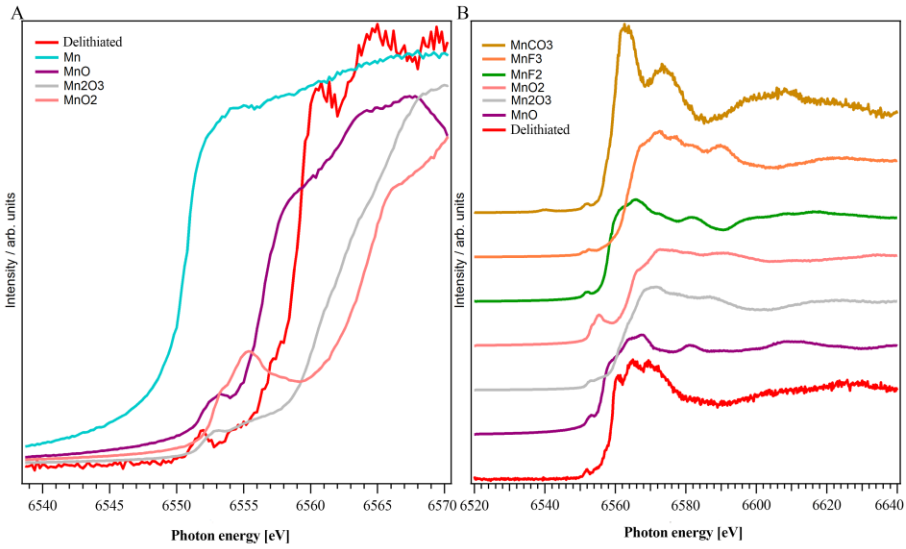

Figure 12. To the left, the absorption-edge of manganese for the samples compared to manganese with known oxidation-states of 0, +I, +II, +III, and +IV. To the right, Mn NEXAFS data for a cycled sample and MnO, Mn_2O_3, MnO_2, MnF_2, MnF_3, and $MnCO_3$ reference spectra.

To investigate if manganese took part in any shuttle mechanisms or otherwise was affected by the electrochemistry during cell operation, NEXAFS measurements were performed on two samples with different degrees of lithiation: completely lithiated and fully delithiated. The absorption edges of the lithiated and delithiated samples are presented in Fig. 13 A. The overall shapes of the post-edge regions were almost identical for both samples; the small variation could originate from difficulties in finding an appropriate background and normalization point. These results would then contradict the suggestions that manganese plays an active role in the degradation processes leading to SEI layer formation. This is further supported by the PES of manganese since there was no observable difference between the manganese spectra for these samples.

In previous studies, the research focus has been on the effect of manganese on graphite anodes rather than on LTO, and little is known about the manganese deposition on LTO. However, the working potential of LTO is below that of manganese reduction, just as for graphite, and therefore all previously proposed mechanisms for graphite could in theory apply also for cells using LTO. To investigate this possibility, a graphite reference cell produced using the same procedures and merely substituting LTO for graphite, was investigated. The resulting NEXAFS data are presented in Fig. 13 B.

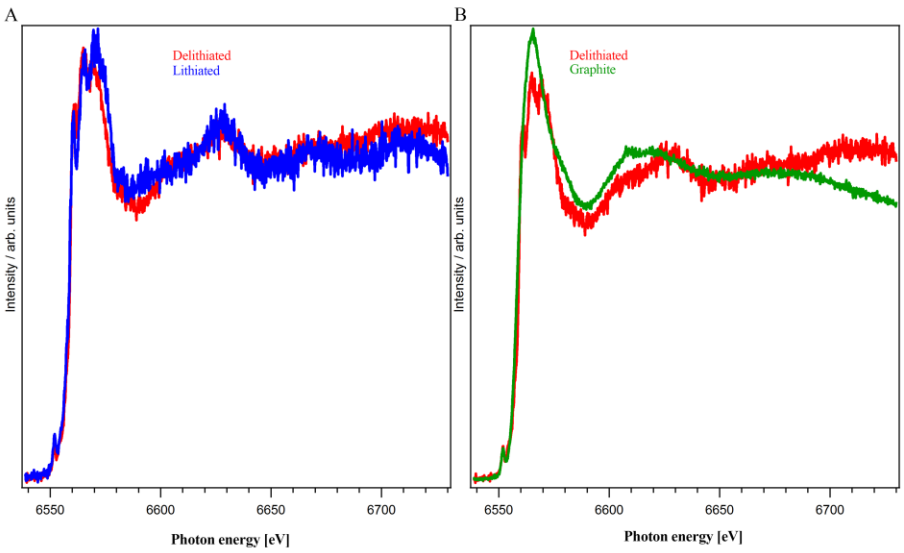

Figure 13. NEXAFS spectra of lithiated and delithiated sample (left) and delithiated sample and graphite reference (right).

Contrary to the comparison between lithiated and delithiated samples, the post edge structure was completely different for the delithiated LTO sample and graphite, indicating that the chemical environment was different for manganese in the two electrode materials. The manganese was, however, still in the same redox state since the absorption edge was positioned at the same energy. Since the NEXAFS result indicates an ionic state of the manganese, this rules out metallic poisoning as a degradation mechanism for both graphite and LTO. However, the difference between LTO and graphite suggests a different SEI forming mechanism, or at least different manganese compounds formed.

4.2.3 Implications of the full-cell investigations

The full-cell data agree with those obtained for the half-cells, indicating a spontaneously formed SEI and a subsequent stripping of this layer during cell cycling. There was manganese present in the SEI of the full-cell, but this manganese appeared to have no profound impact on the composition of the SEI, which is similar to the SEI layer in the half-cell. The manganese was found in the oxidation state of at least +II irrespective of the charging level, which excludes metallic poisoning as an explanation for the accelerated capacity fading of full-cells.

5. Conclusions and future work

This thesis presents an investigation of the interfacial chemistry of LTO electrodes in half-cells and full-cells. The existence of an SEI has been experimentally verified using PES as characterization method. The main components of the SEI are O-C=O, O-C-O/C=O, and P-O species, with the salt decomposition product P-O closest to the surface of the anode. This SEI is different in composition compared to the spontaneously formed surface layer which is comprised of C=O/O-C-O, and P-O as well but which contains carbonates rather than O-C=O bonds and all in different ratios compared to the electrochemically formed SEI. The spontaneously formed surface layer seems to be catalytically driven on the surface of the carbon components in the composite electrode, and this formed SEI layer is stripped from the surface of the anode during electrochemical cycling. While manganese was present in its oxidation state +II to +III in the SEI of LTO in the full-cells with LMO, the manganese does not seem to be altering the SEI composition significantly. The state of manganese was shown to be different with graphite than with LTO, prompting more research to be done on LTO since this material is sparsely investigated. While the complex chemical state of manganese in the SEI layer needs more research to be fully understood, simple explanations such as formation of homogeneous oxides, fluorides, or carbonate can be ruled out.

The LTO material operates at a potential were aluminum alloying with lithium does not occur, which would enable the utilization of aluminum as anode current collector to generate a higher gravimetric capacity as compared to a copper current collector. Moreover, the $LiPF_6$ salt is very prone to decomposition in the environment tested. The LP40 electrolyte has generally been chosen for its outstanding performance with graphite, but LTO presents opportunities for tailoring new electrolytes with improved performances.

For example, lithium bis(trifluoromethanesulfonyl)imide (LiTFSI) is a salt with good properties with respect to thermal and chemical stability, ionic conductivity in many solvents, and resistance to moisture, but which has so far not been implemented on a large scale due to its inability to passivate aluminum current collectors. This could be a very interesting salt to investigate together with LTO. The dissolution of manganese has also proven to be significantly reduced with other salts than $LiPF_6$, and it would be highly

interesting to investigate an LTO-LMO cell containing LiTFSI. Moreover, LiTFSI has been the salt of choice for many solid polymer electrolyte (SPE) systems. SPEs are generally more stable than liquid electrolytes, having wider ESWs and thereby avoiding continuous electrolyte reduction. The LTO/SPE combination could provide a very robust system, making it an interesting choice for long-term cycling applications.

Finally, considering that LTO is investigated for large-scale applications, the environmental aspects become an increasing concern. The PVdF binder is sensitive to moisture and requires the use of organic solvents, which have a higher negative impact on the environment than water. A transition to water soluble binders such as carboxymethyl cellulose (CMC) or polyacrylic acid (PAA) would therefore render the cell manufacturing more environmental friendly. Alternative binders have been explored to a very limited degree for LTO. Future work could well involve evaluations of the electrode performance using water-soluble binders.

6. Sammanfattning på svenska

Den ökande miljömedvetenheten i samhället driver utvecklingen mot mer hållbara alternativ. Energilagring har här en nyckelroll då den tillåter en åtskiljning av energiproduktion och -konsumtion i tid och rymd. Elektrokemisk energilagring har varit känt sedan upptäckten av Voltas stapel år 1800, men det var inte förrän bilindustrins uppkomst som behovet av portabel elektrisk energi kom att växa stort, då med bly-syra batterier för bilarnas startmotorer. Med intåget av mobiltelefoner och laptops följde en vilja att betala för högre energitäthet i batterier för portabla ändamål, och dörren öppnades för en övergång till de dyrare litium-jon-teknologierna. Det första kommersialiserade Li-jonbatteriet (LIB) lanserades av Sony 1991 och mycket jobb har sedan dess lagts ner på att förstå och förbättra det.

Sonys batteri från 1991 byggde på en negativ anod av grafit och en positiv katod av litiumkoboltoxid (LCO), två material av interkalationstyp och konceptet ”gungstols-batteri” var därmed fött. Denna typ av batteri var ett stort lyft i säkerhet jämfört med tidigare litiumbatterier då det minskar risken för dendritbildning och därmed kortslutning som kan leda till termisk rusning och eventuellt en explosion. För grafit kvarstår risken av dendritbildning vid användningsområden med höga strömmar eller i miljöer av med temperaturer, och därför har litiumtitanatoxid (LTO) föreslagits som ett alternativt material till grafit för tillämpningsområden där dessa omständigheter kan förekomma. Ett sådant exempel är för tunga hybridfordon med regenerativ bromsning, vilket är batteritillämpningsområdet av intresse för denna avhandling.

Batterier för dessa tillämpningar kräver mer kapacitet, och därmed volym, än vad Sony utvecklade sitt LIB för 1991. Koboltoxiden som användes som katod i Sonys batteri är dyr och kobolt är toxiskt för miljön och behöver därför bytas ut i batterier för storskalig produktion om dessa skall vara miljövänliga och ekonomiskt hållbara. För detta ändamål har litiummanganoxid (LMO) föreslagits som ersättare för LCO då mangan är mycket vanligare förekommande i jordskorpan därmed möjliggör en mer kostnadseffektiv utvinning. Manganoxiden är dessutom i sig själv ofarlig för miljön.

SEI, från engelskans Solid Electrolyte Interphase, är ett ytlager som bildas på elektroderna i ett batteri. SEI bildas då elektroderna arbetar vid en potential som inte elektrolyten är stabil vid, vilket medför elektronöverföring till elektrolyten så att denna bryts ner. Restprodukterna som bildas utgör det

som kallas för SEI-lagret. SEI-lagret ökar den interna resistansen av ett batteri samt konsumerar litiumjoner, vilket medför minskad kapacitet i batteriet.

LTO opererar vid en högre potential än grafit vilket minskar risken för deponering av metalliskt litium och därmed höjs säkerheten. Av samma skäl har det föreslagits att detta borde göra LTO fritt från SEI, då elektrolyten är stabil vid denna potential.

I denna avhandling har LTO undersökts med den ytkänsliga metoden fotoelektronspektroskopi för att undersöka om LTO verkligen är fritt från SEI. Studierna visade att tillsammans med vanliga elektrolytsystem så kommer det att bildas SEI på LTO även om omfattningen är mindre än på konventionella grafitelektroder. Studierna visade också att SEI-skiktet på LTO består av ett oorganisk lager av produkter från litiumsaltet närmast elektroden, följt av ett organisk lager av elektrolytrester utanpå, allting tunnare än runt 2-3 nanometer tjockt.

Vidare är det sedan tidigare känt att LMO släpper ut mangan i elektrolyten, och det har företagits flera undersökningar för att studera hur detta påverkar SEI-lagret på grafit. I denna avhandling studerades det hur mangan i elektrolyten påverkar SEI på LTO. Resultaten visade att mangan återfinns på ytan av LTO, men att dess närvaro inte påverkar sammansättningen av SEI i någon större utsträckning. Mangan visade ingen skillnad på tillstånd mellan olika elektrokemiska potentialer hos LTO, vilket också indikerar att manganet inte deltar i någon skyttelprocess som påskyndar bildandet av SEI-skiktet. Dessa resultat ger indikationer på vilka kemiska processer som är väsentliga för stabiliteten hos LTO-baserade batterier, och därmed hur dessa skall kunna förbättras.

7. Acknowledgements

There is a long list of persons I would like to extend my gratitude to.

First and foremost I would like to thank my supervisors; Kristina Edström, Daniel Brandell, and Carl Tengstedt. The extreme patience shown towards me and the guidance given is what made this possible. Special thanks to Daniel that even during parental leave continued to give instantaneous feedback on everything I sent and made sure I was on track, something I have to come to not take for granted.

I would like to thank Reza Younesi for all the help, guidance, collaborations, and discussions given throughout the years. I would alongside Reza also thank Maria Hahlin, Julia Maibach, and Chao Xu for helping me navigate in this maze called XPS.

Many thank you to David Rehnlund and Fabian Jeschull for not only the scientific collaborations but also all the fun times outside work.

Thank you Henrik Eriksson for all the help and continuous support in the lab, you were there in the beginning and taught me how to build my first battery.

I would like to thank the "away-team", all of you who made synchrotron visits bearable; Maria, Reza, Julia, Chao, Bertrand Philippe, Fredrik Lindgren, Erik Björklund, Burak Aktekin, Rebecka Lindblad. Mihaela Gorgoi, Roberto Felix Duarte, Maxim Tchaplyguine thank you for keeping the beamlines functioning.

I would like to thank Linus von Fieandt and Johan Cedervall for the time at the office landscape, you made those two years. However brief, I loved sharing office with you guys, Chao and Andreas Blidberg. Thank you Paulius Malinovskis for making the current office the place it is.

I would like to thank "Kaffegruppen" Linus, Johan, Ernesto Vargas, David, Kristina Johansson, Johan Gerdin, Sarmad Katea for all the fun times at and outside work.

Thanks to all the administration current and previous for all help; Eva, Tatti, Anna, Diana, Kristoffer, Slavica, and Jennie.

Many thanks to the battery group and all other working at the office; Adam, Alina, Charlotte, Chenjuan, Gabi, Girma, Habtom, Jonas M., Jonas Å., Mahsa, Mario, Matt, Ocean, Ronnia, Ruijun, Sara, Shruti, Solveig, Stevén, Wei, Viktor, and Will for all discussions and for making the work the place it is.

I would like to thank my parents and my brothers for all the support and encouraging received. I would like to thank my grandparents Nils-Gunnar and Inger Karlsson for always supporting and encouraging my decisions and keeping me fed during my visits home. I would like to thank Solveig Nordh-Thorsell for the help and encouragement I received when setting out on this path.

Thank you All

8. References

1. Tarascon, J. M. & Armand, M. Issues and challenges facing rechargeable lithium batteries. *Nature* **414,** 359–367 (2001).
2. Armand, M. & Tarascon, J.-M. Building better batteries. *Nature* **451,** 652–657 (2008).
3. Nishi, Y. Lithium ion secondary batteries; past 10 years and the future. *J. Power Sources* **100,** 101–106 (2001).
4. Landi, B. J., Ganter, M. J., Cress, C. D., DiLeo, R. A. & Raffaelle, R. P. Carbon nanotubes for lithium ion batteries. *Energy Environ. Sci.* **2,** 638 (2009).
5. Goodenough, J. B. & Kim, Y. Challenges for Rechargeable Li Batteries †. *Chem. Mater.* **22,** 587–603 (2010).
6. Goodenough, J. B. & Kim, Y. Challenges for rechargeable batteries. *J. Power Sources* **196,** 6688–6694 (2011).
7. Goodenough, J. B. & Park, K.-S. The Li-ion rechargeable battery: a perspective. *J. Am. Chem. Soc.* **135,** 1167–76 (2013).
8. Aoshima, T., Okahara, K., Kiyohara, C. & Shizuka, K. Mechanisms of manganese spinels dissolution and capacity fade at high temperature. *J. Power Sources* **98,** 378–381 (2001).
9. Arora, P. & White, R. E. Capacity Fade Mechanisms and Side Reactions in Lithium-Ion Batteries. *J. Electrochem. Soc.* **145,** 3647–3667 (1998).
10. Zhong, Q., Bonakdarpour, A., Zhang, M., Gao, Y. & Dahn, J. R. Synthesis and Electrochemistry of $LiNi_xMn_{2-x}O_4$. *J. Electrochem. Soc.* **144,** 205 (1997).
11. Palacín, M. R. Recent advances in rechargeable battery materials: a chemist's perspective. *Chem. Soc. Rev.* **38,** 2565–75 (2009).
12. Ferg, E. Spinel Anodes for Lithium-Ion Batteries. *J. Electrochem. Soc.* **141,** L147 (1994).
13. Ohzuku, T. Zero-Strain Insertion Material of $Li[Li1_{/3}Ti_{5/3}]O_4$ for Rechargeable Lithium Cells. *J. Electrochem. Soc.* **142,** 1431 (1995).
14. Jansen, A. . *et al.* Development of a high-power lithium-ion battery. *J. Power Sources* **81-82,** 902–905 (1999).
15. Christensen, J., Srinivasan, V. & Newman, J. Optimization of Lithium Titanate Electrodes for High-Power Cells. *J. Electrochem. Soc.* **153,** A560 (2006).

16. Kalhoff, J., Eshetu, G. G., Bresser, D. & Passerini, S. Safer Electrolytes for Lithium-Ion Batteries: State of the Art and Perspectives. *ChemSusChem* **8,** 2154–2175 (2015).
17. Vetter, J. *et al.* Ageing mechanisms in lithium-ion batteries. *J. Power Sources* **147,** 269–281 (2005).
18. Winter, M. & Brodd, R. J. What are batteries, fuel cells, and supercapacitors? *Chem. Rev.* **104,** 4245–4269 (2004).
19. Kanevskii, L. S. & Dubasova, V. S. Degradation of lithium-ion batteries and how to fight it: A review. *Russ. J. Electrochem.* **41,** 1–16 (2005).
20. Verma, P., Maire, P. & Novák, P. A review of the features and analyses of the solid electrolyte interphase in Li-ion batteries. *Electrochim. Acta* **55,** 6332–6341 (2010).
21. Kitta, M., Akita, T., Maeda, Y. & Kohyama, M. Study of surface reaction of spinel $Li_4Ti_5O_{12}$ during the first lithium insertion and extraction processes using atomic force microscopy and analytical transmission electron microscopy. *Langmuir* **28,** 12384–92 (2012).
22. El Ouatani, L., Dedryvère, R., Siret, C., Biensan, P. & Gonbeau, D. Effect of Vinylene Carbonate Additive in Li-Ion Batteries: Comparison of $LiCoO_2$/C, $LiFePO_4$/C, and $LiCoO_2$/$Li_4Ti_5O_{12}$ Systems. *J. Electrochem. Soc.* **156,** A468 (2009).
23. Dedryvère, R. *et al.* Electrode/electrolyte interface reactivity in high-voltage spinel $LiMn_{1.6}Ni_{0.4}O_4$/$Li_4Ti_5O_{12}$ lithium-ion battery. *J. Phys. Chem. C* **114,** 10999–11008 (2010).
24. He, Y. B. *et al.* Carbon coating to suppress the reduction decomposition of electrolyte on the $Li_4Ti_5O_{12}$ electrode. *J. Power Sources* **202,** 253–261 (2012).
25. He, Y.-B. *et al.* Gassing in $Li_4Ti_5O_{12}$-based batteries and its remedy. *Sci. Rep.* **2,** 913 (2012).
26. He, Y. B. *et al.* Effect of solid electrolyte interface (SEI) film on cyclic performance of $Li_4Ti_5O_{12}$ anodes for Li ion batteries. *J. Power Sources* **239,** 269–276 (2013).
27. Belharouak, I. *et al.* Performance Degradation and Gassing of $Li_4Ti_5O_{12}$/$LiMn_2O_4$ Lithium-Ion Cells. *J. Electrochem. Soc.* **159,** A1165–A1170 (2012).
28. Borgel, V., Gershinsky, G., Hu, T., Theivanayagam, M. G. & Aurbach, D. $LiMn_{0.8}Fe_{0.2}PO_4$/$Li_4Ti_5O_{12}$, a Possible Li-Ion Battery System for Load-Leveling Application. *J. Electrochem. Soc.* **160,** A650–A657 (2013).
29. Song, M.-S. *et al.* Is $Li_4Ti_5O_{12}$ a solid-electrolyte-interphase-free electrode material in Li-ion batteries? Reactivity between the $Li_4Ti_5O_{12}$ electrode and electrolyte. *J. Mater. Chem. A* **2,** 631 (2014).
30. Jang, D. H., Shin, Y. J. & Oh, S. M. Dissolution of Spinel Oxides and Capacity Losses in 4 V Li/$Li_xMn_2O_4$ Cells. *J. Electrochem. Soc.* **143,** 2204 (1996).

31. Blyr, A. Self-Discharge of $LiMn_2O_4$/C Li-Ion Cells in Their Discharged State. *J. Electrochem. Soc*. **145,** 194 (1998).
32. Tsunekawa, H. *et al.* Capacity Fading of Graphite Electrodes Due to the Deposition of Manganese Ions on Them in Li-Ion Batteries. *J. Electrochem. Soc*. **149,** A1326 (2002).
33. Amine, K. *et al.* Improved lithium manganese oxide spinel/graphite Li-ion cells for high-power applications. *J. Power Sources* **129,** 14–19 (2004).
34. Yang, L., Takahashi, M. & Wang, B. A study on capacity fading of lithium-ion battery with manganese spinel positive electrode during cycling. *Electrochim. Acta* **51,** 3228–3234 (2006).
35. Ochida, M. *et al.* Influence of Manganese Dissolution on the Degradation of Surface Films on Edge Plane Graphite Negative-Electrodes in Lithium-Ion Batteries. *J. Electrochem. Soc.* **159,** A961–A966 (2012).
36. Zhan, C. *et al.* Mn(II) deposition on anodes and its effects on capacity fade in spinel lithium manganate-carbon systems. *Nat. Commun*. **4,** 2437 (2013).
37. Delacourt, C. *et al.* Effect of Manganese Contamination on the Solid-Electrolyte-Interphase Properties in Li-Ion Batteries. *J. Electrochem. Soc*. **160,** A1099–A1107 (2013).
38. Lu, D., Xu, M., Zhou, L., Garsuch, A. & Lucht, B. L. Failure Mechanism of Graphite/$LiNi_{0.5}Mn_{1.5}O_4$ Cells at High Voltage and Elevated Temperature. *J. Electrochem. Soc*. **160,** A3138–A3143 (2013).
39. Gowda, S. R. *et al.* Oxidation state of cross-over manganese species on the graphite electrode of lithium-ion cells. *Phys. Chem. Chem. Phys*. **16,** 6898–902 (2014).
40. Shkrob, I. A. *et al.* Manganese in Graphite Anode and Capacity Fade in Li Ion Batteries. *J. Phys. Chem. C* **118,** 24335–24348 (2014).
41. Xiao, X. *et al.* Unraveling manganese dissolution/deposition mechanisms on the negative electrode in lithium ion batteries. *Phys. Chem. Chem. Phys*. **16,** 10398–402 (2014).
42. Shin, H., Park, J., Sastry, A. M. & Lu, W. Degradation of the solid electrolyte interphase induced by the deposition of manganese ions. *J. Power Sources* **284,** 416–427 (2015).
43. Einstein, A. Generation and conversion of light with regard to a heuristic point of view. *Ann. Phys*. **17,** 132–148 (1905).
44. J. F. Moulder, Handbook of X-Ray Photoelectron Spectroscopy, 1995
45. S. Hüfner, NEXAFS Spectroscopy, 1992
46. Ciosek Högström, K. *et al.* The influence of PMS-additive on the electrode/electrolyte interfaces in $LiFePO_4$/graphite li-ion batteries. *J. Phys. Chem. C* **117,** 23476–23486 (2013).
47. Younesi, R., Hahlin, M. & Edström, K. Surface characterization of the carbon cathode and the lithium anode of Li-O_2 batteries using

$LiClO_4$ or LiBOB salts. *ACS Appl. Mater. Interfaces* (2013). doi:10.1021/am3026129

48. Lin, X. *et al.* A Comprehensive Capacity Fade Model and Analysis for Li-Ion Batteries. *J. Electrochem. Soc.* **160,** A1701–A1710 (2013).
49. Clark, D. T., Dilks, A., Thomas, H. R., Shuttleworth, D. & Al, C. E. T. ESCA Applied to Polymers . XXII . An Investigation of Sample Charging Phenomena for Polymeric Films on Gold. *J. Polym. Sci. Polym. Chem. Ed.* **17,** 627–638 (1979).
50. Choi, W. & Manthiram, A. Comparison of Metal Ion Dissolutions from Lithium Ion Battery Cathodes. *J. Electrochem. Soc.* **153,** A1760 (2006).